

Path Integral Calculations of the Hydrogen Hugoniot Using Augmented Nodes

Saad A. Khairallah,^{1,*} J. Shumway,^{2,†} and Erik W. Draeger¹

¹*Lawrence Livermore National Laboratory, Livermore, CA 94550*

²*Department of Physics, Arizona State University, Tempe AZ 85287*

(Dated: August 9, 2011)

We calculate the hydrogen Hugoniot using ab initio path integral Monte Carlo. We introduce an efficient finite-temperature fixed-node approximation for handling fermions, which includes an optimized mixture of free particle states and atomic orbitals. The calculated Hugoniot confirms previous fixed-node path integral calculations at temperatures around $T = 30\,000$ K and above, while approaching smoothly the low temperature gas gun results. The ability to optimize the free energy within the path integral opens many new possibilities for developing nodal density matrices for path integral simulations of other chemical systems.

PACS numbers: 62.50.+p, 02.70.Lq, 05.30.-d

Predicting the properties of materials at extreme conditions of high pressures and high temperatures is a fundamental challenge in computational physics, particularly when quantum effects are significant. One such system is the hydrogen Hugoniot, measured in laser shock-wave [1, 2] and gas gun [3] experiments, which has become one of the benchmarks for state-of-the-art theory.

Path Integral Monte Carlo (PIMC) allows direct calculation of thermodynamic properties of many-body quantum systems at finite temperature [4–10]. For fermions, an additional “fixed-node” constraint is imposed to prevent an exponential slowdown in convergence with increasing system size and decreasing temperature [11, 12]. This requirement to supply an *a priori* form for the nodal surface of the many-body wavefunction has limited the application of PIMC almost exclusively to hydrogen and helium systems at high temperatures. Not only does the use of an approximate nodal function introduce uncontrolled error, traditional algorithms for enforcing the nodal constraint have been shown to become increasingly inefficient at lower temperatures, ultimately failing to satisfy the Monte Carlo ergodicity requirement. For hydrogen, nodal errors begin to manifest at lower temperatures, below $100\,000$ K [7], and ergodicity becomes difficult to achieve below $20\,000$ K [7].

In this Letter, we present a simplifying approximation to fixed-node PIMC that resolves several of these issues. This new implementation is fully symmetric in imaginary time, thus achieving better computational efficiency in addition to avoiding the ergodicity issues of the traditional approach. More importantly, the method allows the relative free energies of different nodal choices to be sampled directly within PIMC simulations, *thus providing a systematic way to construct an optimal nodal function*. This is an important independent verification of other ab initio proposals and brings the benefits of PIMC to a much broader physical domain. While the ability to test and improve nodes using total energies has been common in ground-state Quantum Monte Carlo (QMC), extending practical tests of nodes to compare free ener-

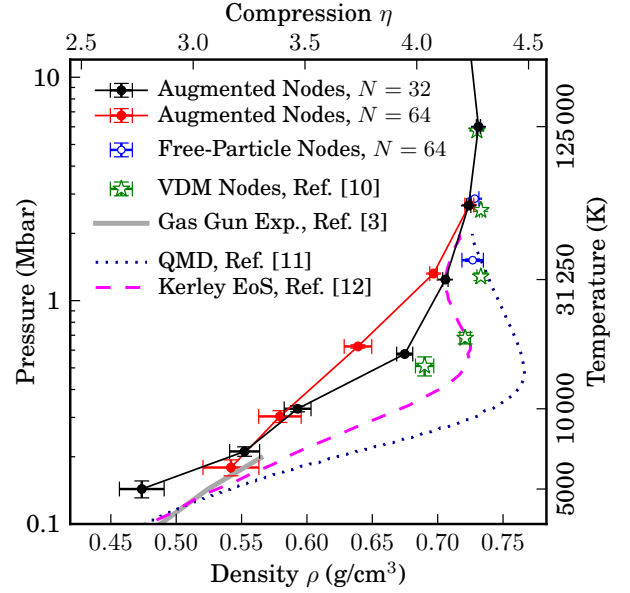


FIG. 1. (color online) The Deuterium Hugoniot curve calculated within PIMC from $T = 125\,000$ K down to $T = 5\,000$ K. While free particle nodes are sufficient at high temperatures (above $125\,000$ K, see Table I), augmented nodes are necessary once bound electronic states form. Our Hugoniot curve approaches the correct free particle limit of fourfold compression in the high temperature and pressure limit (not shown).

gies is an important advancement in the study of finite temperature nodes. This could have far-reaching consequences, as atomic and molecular orbitals can be introduced without bias, potentially paving the way to extend PIMC to heavier elements and lower temperatures.

We demonstrate the new formalism with calculations of the hydrogen Hugoniot (Fig. 1), using augmented nodes incorporating $1s$ atomic orbitals. Our calculations of the hydrogen Hugoniot span temperatures from $T = 1\,000\,000$ K all the way down to $5\,000$ K, overlapping for the first time with ground state theories like Density Functional Theory (DFT) [13, 14], as well as lower-

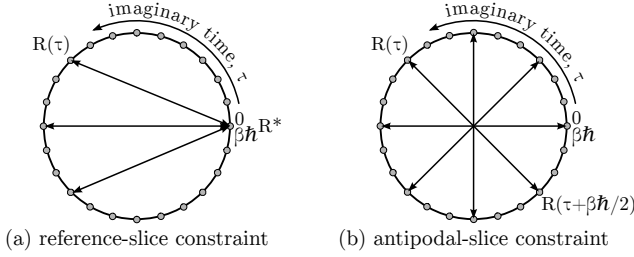


FIG. 2. Schematic illustration of the (a) reference-slice fixed-node, Eq. (2), [11] and (b) antipodal-slice fixed-node, Eq. (3), constraints for path integrals.

temperature gas gun experiments [3]. There is a general consensus over the high and low pressure limits of the Hugoniot curve. A controversy arises at the intermediate pressure, around 1 Mbar, where laser-driven shock measurements [1] observe high compression $\eta \sim 5.5 - 6$ while magnetically driven flyers [15] and convergent explosives [16] find a stiffer curve closer to $\eta \sim 4$. We agree with the latter with a maximum compression measurement $\eta \sim 4.2$. We see no evidence of a plasma phase transition that has been predicted by some other simulations [17, 18]. Our results are consistent with recent QMC and DFT calculations that show that a metal-insulator phase transition occurs only stakes place at lower temperatures, below 2000 K, at pressures above 1.2 Mbar [19, 20].

PIMC uses Feynman's path integral formulation of statistical mechanics to describe a quantum system in thermal equilibrium with a path integral over imaginary time:

$$\langle R | e^{-\beta H} | R' \rangle = \int_{\substack{R(\beta\hbar) = R \\ R(0) = R'}} \mathcal{R}(\tau) e^{-\frac{1}{\hbar} S_E[R(\tau)]}, \quad (1)$$

where R represents all the particle coordinates, and the path $R(\tau)$ extends for an imaginary time $\beta\hbar = \hbar/k_B T$. In PIMC simulations, the path is discretized into N_T slices, where N_T is the Trotter number, which divides imaginary time into short imaginary-time intervals, $\Delta\tau = \beta\hbar/N_T$. To handle fermions, the path integral, Eq. (1), is antisymmetrized over all permutations of identical particles, which leads to an exponential decrease in algorithmic efficiency at low temperatures and large system sized, known as the fermion sign problem.

One strategy to manage the fermion sign problem is the fixed-node approximation. The traditional implementation of the fixed-node approximation restricts the path integral to paths that satisfy the constraint [11],

$$\rho_T(R(\tau), R^*; |\tau|) > 0 \quad (\forall \tau \in [-\beta\hbar/2, \beta\hbar/2]), \quad (2)$$

where the reference slice coordinates are taken at $\tau = 0$ so that $R^* = R(0)$, as shown in Fig. 2(a). This rigorously enforces the nodal constraint, but adds imaginary-time dependence to the evaluation of the nodal action [11]. The nodal model ρ_T must be defined for imaginary times

ranging from $\Delta\tau$ to $\beta\hbar/2$, corresponding to temperatures ranging from $2T$ to $N_T T$.

In the antipodal slice approach, we make a simplifying approximation,

$$\rho_T(R(\tau), R(\tau + \beta\hbar/2)) \neq 0 \quad (\forall \tau \in [-\beta\hbar/2, 0]), \quad (3)$$

illustrated in Fig. 2(b). For each slice $R(\tau)$, we evaluate the constraint with the slice $R(\tau + \beta\hbar/2)$ that is antipodal to the slice, rather than the reference slice R^* . While we have tested this constraint on many problems, we have not determined its range of validity; the results presented here are a pragmatic test of the antipodal approximation. By lifting the imaginary-time dependence, the antipodal slice approximation allows one to avoid ergodicity errors caused by the reference slice getting “pinned” at lower temperatures where the number of imaginary-time slices N_T becomes large and long permutation cycles become increasingly common. The nodal model is greatly simplified, as ρ_T now only needs to be evaluated at one temperature $2T$ for the imaginary time $\tau = \beta\hbar/2$. Parallel scalability is similarly increased, as antipodal collections of slices can simultaneously make multiple multilevel moves [4] on local processors without requiring global communication.

The most significant advancement allowed by the antipodal approximation, however, is the ability to directly compare the free energies of different nodal models. We hypothesize that the best nodal choice will be the lowest free energy, in analogy to the best ground state wavefunction nodes having the lowest energy. For the nodal density matrix, we take a product of Slater determinants,

$$\rho_T(R, R') = \det |\rho(\mathbf{r}_{i\uparrow}, \mathbf{r}_{j\uparrow})| \det |\rho(\mathbf{r}_{i\downarrow}, \mathbf{r}_{j\downarrow})|, \quad (4)$$

where $\rho(\mathbf{r}, \mathbf{r})$ are single-particle density matrices at a temperature $T/2$. In this work we augment the single particle density matrices by including a hydrogen 1s orbital in the thermal mixture,

$$\rho(\mathbf{r}, \mathbf{r}'; \beta, w) = \frac{\exp\left(-\frac{m|\mathbf{r}_i - \mathbf{r}'_j|^2}{2\beta\hbar^2}\right)}{(2\pi\beta\hbar^2/m)^{3/2}} + w \sum_k^{N_{\text{ion}}} \psi_{1s}(\mathbf{r}_i - \mathbf{r}'_j) \psi_{1s}^*(\mathbf{r}'_j - \mathbf{r}_k) \quad (5)$$

where the weight w is a free parameter and $\psi_{1s}(\mathbf{r})$ is the normalized hydrogen 1s orbital. Here the first term is the free particle thermal density matrix, and the sum is a mixture of density matrices for hydrogenic orbitals about each of the ions, each with a weight w .

To find the optimal value of w , we histogram free energy differences for nodes with different values of w using the acceptance ratio method [21], as shown in Fig. 3. At $T = 62\,500$ K a value of w around 4.7 increases the partition function by about a factor of four. Note that the

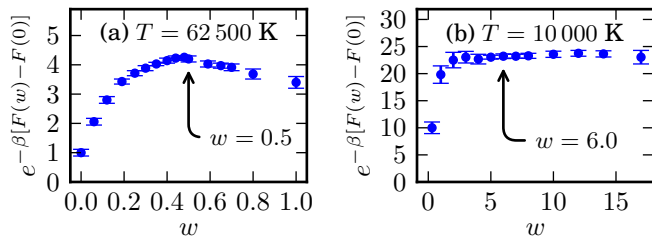


FIG. 3. (color online) The relative partition function $Z \propto \exp(-\beta F[\rho_T(R, R'; T, w)])$ for the system with $r_s = 2.0$, for different nodal choices. The fixed-node free energy $F[\rho_T]$ is a functional of the nodal density matrix, ρ_T . The parameter w is the weight of the 1s orbital in the augmented nodal mixture, Eq. (5). At higher temperatures, there is a clear maximum in the free energy, while the free energy saturates for large values of w at low temperatures. Arrows indicate optimal values of w , and we report all choices of w in Table I.

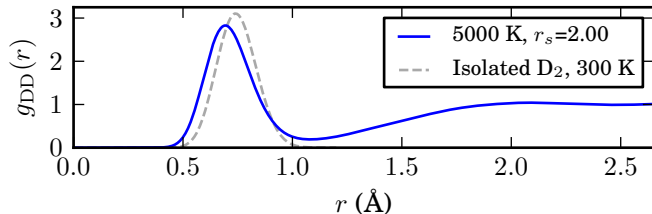


FIG. 4. (color online) The pair correlation function $g(r)$ for 32 deuterium atoms at $T = 5000$ K, computed using PIMC with augmented nodes. The contribution to $g(r)$ from an isolated molecule at 300 K is shown for comparison, illustrating the compression of the molecules.

partition function decreases for larger values of w , indicating an optimal mixture of atomic 1s and free particle density matrices occurs near $w = 5$. At $T = 10\,000$ a value of w around 3 or larger increases the partition function by more than a factor of 20. The partition function is relatively insensitive to w for all $w > 3$, indicating that the 1s orbitals dominate the nodal surface.

Such a systematic approach for optimizing a given nodal model from first principles has not been possible before within the reference slice approach, due to the fact that the nodes are time-dependent and require a complete set of terms over the full range of inter-slice temperatures from MT down to $2T$. We note that this is analogous to optimizing ground nodes directly diffusion Monte Carlo energies, which is the most rigorous ground state fixed-node strategy [22, 23].

To allow direct comparison with traditional reference slice PIMC, we performed calculations of the hydrogen Hugoniot using the same densities as Ref. 7. We ran periodic simulation with $N = 32$ and $N = 64$ deuterium atoms and for both densities with $r_s = 2.00$ and $r_s = 1.86$. Following Ref. 7, we identify the Hugoniot curve by linear interpolation. The two densities accu-

rately bracket the Hugoniot curve at higher pressures, but was found to introduce an extrapolation error at the lowest pressures, making the statistical error bars shown in Fig. 1 a lower bound only. Following the guidance in Ref. 7 on the importance of small time steps, we used $\Delta\tau/\hbar = 0.02 \text{ Ha}^{-1}$, a time step at least twice as small as Ref. 7. Our results are summarized in Fig. 1 and Table I.

In the high temperature and pressure limit, our Hugoniot approaches the correct free particle limit of four-fold compression. We see excellent agreement with past PIMC results at high temperatures and pressures [7], where permutations are infrequent and free particle nodes accurately describe a dense strongly interacting plasma. An augmented node description starts becoming necessary below 62 500 K, resulting in lower free energy than free particle nodes alone. Using augmented nodes, we see the Hugoniot curving towards lower compression in the 1 Mbar regime, before eventually coming closer to gas-gun and DFT low pressure results [3, 24]. We note that the antipodal slice approximation also speeds up simulations considerably, as we find that parallel simulations run more than four times faster in direct comparisons to reference-slice fixed-node simulations.

We note that these results differ somewhat from the lowest pressure results of Ref. [7], which used a variational approach to optimize the parameters in a density matrix assumed to be a Slater determinant of Gaussians. The variational nodes are shown to give lower energies than the free particle density matrix in Ref. 7, however, no formal proof is given that variational nodes used there result in the lowest free energy. Further investigation is needed to resolve this discrepancy. We note that using 1s orbitals in our augmented node results is also a crude model that can be enhanced by adding higher orbitals.

Our results do not seem to suffer from finite size effects at higher temperatures. This is not the case at low temperatures. We comment on the exceptional discrepancy at $T = 15\,625$ K. This is where DFT-MD shows some difficulty probing the simultaneous molecular bonding and dissociations that take place in this range. DFT which can be notorious in describing bond lengths and band gap closure could be exaggerating a high compression trend. Long distance correlations and delocalized electron paths are observed in our PIMC simulations. This may suggest the need for larger PIMC simulation box size and more atoms to account for these correlations.

We note that in the direct PIMC approach by [18], the PIMC simulations did not seem to converge to an equilibrium state around 10 000 K, and a plasma transition into partially ionized deuterium was assumed to take place in that region. A notable configurational expression of this is the nuclei form metallic clusters (droplets) with highly delocalized electrons over them [18]. We do not observe this behavior in our simulation.

Our data are within error bars of the magnetically driven flyer [15] and convergent explosive [16] experi-

TABLE I. PIMC calculation of deuterium Hugoniot and compressibilities with respect to an initial cryogenic state of 0.171 g/cc at $T = 19.6$ K. A small time step of $\tau^{-1} = 1.536 \times 10^7$ K ($\Delta\tau/\hbar = 0.02$ Ha $^{-1}$, twice smaller than Ref. [7]) is used.

T(K)	p (Mbar) $r_s = 2$	E (eV) $r_s = 2$	w $r_s = 2$	p (Mbar) $r_s = 1.86$	E (eV) $r_s = 1.86$	w $r_s = 1.86$	p (Mbar) Hugoniot	ρ (g/cm 3) Hugoniot	η Hugoniot
1 000 000	54.14(3)	245.2(1)	0.	67.35(5)	244.6(2)	0.	56.51(3)	0.7028(3)	4.110(2)
500 000	26.19(2)	113.1(1)	0.	32.46(2)	111.9(1)	0.	27.74(1)	0.7138(4)	4.174(2)
250 000	12.24(1)	45.8(1)	0.	15.18(2)	44.8(1)	0.	13.16(1)	0.7249(6)	4.239(4)
125 000	5.50(2)	12.4(1)	0.	6.94(2)	11.9(1)	0.	6.01(1)	0.7310(2)	4.275(1)
62 500	2.430(19)	-3.44(8)	0.5	3.232(27)	-3.29(10)	0.5	2.677(15)	0.724(4)	4.24(2)
31 250	1.269(8)	-9.76(3)	0.8	1.650(17)	-10.00(6)	0.75	1.322(7)	0.697(3)	4.08(2)
15 625	0.575(5)	-13.26(3)	3.0	0.713(9)	-13.33(3)	0.6	0.577(5)	0.675(6)	3.95(4)
10 000	0.394(5)	-14.55(2)	16.0	0.517(7)	-14.48(2)	6.0	0.306(10)	0.556(15)	3.25(9)
7 813	0.336(5)	-15.04(2)	8.5	0.504(7)	-15.05(3)	8.0	0.211(10)	0.552(12)	3.23(7)
5 000	0.219(4)	-15.72(2)	11.0	0.281(7)	-16.03(2)	9.0	0.143(12)	0.475(18)	2.77(11)

ments. If the recent correction on the equation of state of the quartz standard [25] is taken into account, the laser data shifts to lower compressions indicating that Hydrogen is not as compressible as the older data suggested.

In summary, we present a new time-independent formalism for fixed-node fermionic PIMC which is significantly more efficient and free of the ergodicity issues that plague the traditional reference slice approach. A clear strategy for creating nodal models with lower free energy emerges from this approach, which we anticipate will open the door to systems previously inaccessible to PIMC, including elements with $Z > 2$. We present updated results on the hydrogen Hugoniot which show a clear trend toward the lower compression and closer agreement with Kerley's equation of state [26].

We are thankful for the fruitful discussions with David Ceperley, Kevin Schmidt, Michael Bonitz, Ken Esler, Brian Clark, Jonathan Dubois, Heather Whitley and Bernie Alder. This work was performed under the auspices of the U.S. Department of Energy by Lawrence Livermore National Laboratory under Contract DE-AC52-07NA27344. We also acknowledge financial support from NSF DMR 02-39819.

* khairallah1@llnl.gov

† john.shumway@asu.edu; <http://shumway.physics.asu.edu>

- [1] L. B. Da Silva, P. Celliers, G. W. Collins, K. S. Budil, N. C. Holmes, T. W. Barbee Jr., B. A. Hammel, J. D. Kilkenny, R. J. Wallace, M. Ross, R. Cauble, A. Ng, and G. Chiu, Phys. Rev. Lett., **78**, 483 (1997).
- [2] G. W. Collins, L. B. Da Silva, P. Celliers, D. M. Gold, M. E. Foord, R. J. Wallace, A. Ng, S. V. Weber, K. S. Budil, and R. Cauble, Science, **281**, 1178 (1998).
- [3] W. J. Nellis, A. C. Mitchell, M. van Thiel, G. J. Devine, R. J. Trainor, and N. Brown, The Journal of Chemical Physics, **79**, 1480 (1983).
- [4] D. M. Ceperley, Rev. Mod. Phys, **67**, 279 (1995).
- [5] C. Pierleoni, D. M. Ceperley, B. Bernu, and W. R. Magro, Phys. Rev. Lett., **73**, 2145 (1994).
- [6] W. R. Magro, D. M. Ceperley, C. Pierleoni, and B. Bernu, Phys. Rev. Lett., **76**, 1240 (1996).
- [7] B. Militzer and D. M. Ceperley, Phys. Rev. Lett., **85**, 1890 (2000).
- [8] B. Militzer, D. M. Ceperley, J. D. Kress, J. D. Johnson, L. A. Collins, and S. Mazevet, Phys. Rev. Lett., **87**, 275502 (2001).
- [9] B. Militzer, Phys. Rev. B, **79** (2009).
- [10] S. X. Hu, B. Militzer, V. N. Goncharov, and S. Skupsky, Phys. Rev. Lett., **104**, 235003 (2010).
- [11] D. M. Ceperley, Phys. Rev. Lett., **69**, 331 (1992).
- [12] D. M. Ceperley, in *Monte Carlo and Molecular Dynamics of Condensed Matter Systems*, edited by K. Binder and G. Ciccotti (Editrice Bologna, 1996).
- [13] M. P. Desjarlais, Phys. Rev. B, **68**, 064204 (2003).
- [14] S. A. Bonev, B. Militzer, and G. Galli, Phys. Rev. B, **69**, 014101 (2004).
- [15] M. D. Knudson, D. L. Hanson, J. E. Bailey, C. A. Hall, J. R. Asay, and W. W. Anderson, Phys. Rev. Lett., **87**, 225501 (2001).
- [16] S. Belov, G. Boriskov, A. Bykov, R. Il'kaev, N. Luk'yanov, A. Matveev, O. Mikhailova, V. Selemir, G. Simakov, R. Trunin, I. Trusov, V. Urlin, V. Fortov, and A. Shuikin, JETP Letters, **76**, 433 (2002).
- [17] V. Filinov, V. Fortov, M. Bonitz, and P. Levashov, JETP Letters, **74**, 384 (2001).
- [18] V. Bezukrovniy, V. S. Filinov, D. Kremp, M. Bonitz, M. Schlages, W. D. Kraeft, P. R. Levashov, and V. E. Fortov, Phys. Rev. E, **70**, 057401 (2004).
- [19] M. A. Morales, C. Pierleoni, E. Schwegler, and D. M. Ceperley, Proc. Nat. Acad. Sci. USA, **107**, 12799 (2010).
- [20] W. Lorenzen, B. Holst, and R. Redmer, Phys. Rev. B, **82**, 195107 (2010).
- [21] C. H. Bennett, J. Comp. Phys., **22**, 245 (1976).
- [22] C. J. Umrigar, J. Toulouse, C. Filippi, S. Sorella, and R. G. Hennig, Phys. Rev. Lett., **98**, 110201 (2007).
- [23] F. A. Reboredo, R. Q. Hood, and P. R. C. Kent, Phys. Rev. B, **79**, 195117 (2009).
- [24] L. Caillabet, S. Mazevet, and P. Loubeyre, Phys. Rev. B, **83**, 094101 (2011).
- [25] M. D. Knudson and M. P. Desjarlais, Phys. Rev. Lett., **103**, 225501 (2009).
- [26] G. I. Kerley, *Equations of State for Hydrogen and Deuterium*, Tech. Rep. SAND2003-3613 (Sandia National Laboratories, 2003).